Experimental reconstruction of excitation energies of primary hot isotopes in heavy ion collisions near the Fermi energy

M. R. D. Rodrigues,[1] W. Lin,[2,3] X. Liu,[2,3] M. Huang,[2] S. Zhang,[2,3] Z. Chen,[2] J. Wang,[2] R. Wada,[2,*] S. Kowalski,[4] T. Keutgen,[5] K. Hagel,[6] M. Barbui,[6] C. Bottosso,[6] A. Bonasera,[6,7] J. B. Natowitz,[6] T. Materna,[6] L. Qin,[6] P. K. Sahu,[6] and K. J. Schmidt[4,6]

[1]*Instituto de Física, Universidade de São Paulo, Caixa Postal 66318, CEP 05389-970, São Paulo, Brazil*

[2]*Institute of Modern Physics, Chinese Academy of Sciences, Lanzhou 730000, China*

[3]*University of Chinese Academy of Sciences, Beijing 100049, China*

[4]*Institute of Physics, Silesia University, Katowice, Poland*

[5]*FNRS and IPN, Université Catholique de Louvain, B-1348 Louvain-Neuve, Belgium*

[6]*Cyclotron Institute, Texas A&M University, College Station, Texas 77843, USA*

[7]*Laboratori Nazionali del Sud, INFN, via Santa Sofia 62, 95123 Catania, Italy*

(Received 11 April 2013; revised manuscript received 17 July 2013; published 12 September 2013)

The excitation energies of the primary hot isotopes in multifragmentation events are experimentally reconstructed in the reaction system ^{64}Zn + ^{112}Sn at 40 MeV/nucleon. A kinematical focusing method is employed to evaluate the multiplicities of the evaporated light particles associated with isotopically identified fragments with $3 \leqslant Z \leqslant 14$. Angular distributions of the velocity spectra of light charged particles and neutrons associated with trigger isotopes are examined. A moving source fit is used to separate the kinematically correlated particles, evaporated from the parents of the detected isotopes, from the uncorrelated particles originating from other sources. The latter are evaluated experimentally relative to those in coincidence with the Li isotopes. A parameter, k, is used to adjust the yield of the uncorrelated particles for different trigger isotopes. For each experimentally detected isotope, the multiplicities, apparent temperatures, and k values for n, p, d, t, and α particles are extracted. Using the extracted values, the excitation energies of the primary hot isotopes are reconstructed employing a Monte Carlo method. The extracted excitation energies are in the range of 1 to 4 MeV/nucleon but show a significant decreasing trend as a function of A for a given Z of the isotopes. The results are compared with those of antisymmetrized molecular dynamics (AMD) and statistical multifragmentation model (SMM) simulations. While some of the experimental characteristics are predicted partially by each model, neither simulation reproduces the overall characteristics of the experimental results.

DOI: 10.1103/PhysRevC.88.034605 PACS number(s): 25.70.Mn, 25.70.Pq

I. INTRODUCTION

In central heavy ion collisions at intermediate energies, the composite system formed at an early stage of the reaction is compressed and excited. This hot dense nuclear system expands and can break into fragments by a multifragmentation process. In general the process can be divided into stages: the dynamical compression and expansion, the formation of fragments, and finally the separation and secondary cooling by evaporation. An accurate modeling of these processes is not simple. Global features of the characteristic experimental observables, such as multiplicities, mass or charge distributions, and energy spectra or the mean energy of the fragments, have been well reproduced by both statistical multifragmentation models, such as microcanonical Metropolitan Monte Carlo model (MMMC) [1,2] and the statistical multifragmentation model (SMM) [2–10], and by transport-based models, such as antisymmetrized molecular dynamics (AMD) [11–18], stochastic mean field model (SMF) [19–21], and Improved quantum statistical model (ImQMD) [22–26], although they are based on quite different assumptions. The statistical models utilize a freeze-out concept. The fragmenting system—characterized by size, neutron/proton ratio, excitation energy, and density—is assumed to be in chemical and thermal equilibrium. In recent analyses the parameters are optimized to reproduce the experimental observables of the final state. The transport models do not assume any chemical or thermal equilibrium. Nucleon trajectories are solved classically in the given mean field. Nucleon-nucleon collisions are taken into account stochastically and Pauli-blocking effects are introduced approximately or in an exact manner. Since both methods reproduce many experimental observables equally well, attempts were made to understand theoretical connections between the two. In these attempts reaction and statistical ensembles are generated separately and compared with each other. Raduta *et al*. compared results from SMF and a microcanonical multifragmentation model [27,28]. In these works. they evaluated the reaction ensembles at freeze-out times near 240 fm/c and found an equivalent ensemble in the statistical model. They also pointed out that the thermal equilibration may occur at an earlier time such as 140 to 185 fm/c, depending on the reaction systems studied. Furuta *et al*. [29] made similar comparisons using the same AMD code to generate both the reaction and the statistical ensembles in order to reduce the model dependence. The reaction ensembles were generated for a ^{40}Ca + ^{40}Ca) reaction at 35 MeV/nucleon. The statistical ensembles were generated placing ^{36}Ar in a given box and allowing the system to come to equilibrium. By

*wada@comp.tamu.edu

changing the initial excitation energy, different temperature ensembles are obtained. For each reaction ensemble at a given reaction time (from 80 to 300 fm/c), they were able to identify an equivalent statistical ensemble which has similar charge and excitation energy distributions. One should note that these comparisons provide a necessary but not sufficient condition. For thermal and chemical equilibration, Liu *et al.* studied the average energy of intermediate mass fragment (IMF) isotopes in central collisions of ^{112}Sn + ^{112}Sn reactions at 50 MeV/nucleon [30]. They studied the isotopes with $Z \leqslant 10$, which were emitted around $\theta_{cm} \sim 90^o$. They found that the average energies of isotopes with $Z = N - 1$ are much larger than that of $N \geqslant Z$ isotopes. This difference is much larger than that expected in emission from a thermally equilibrated system. From the comparison with results of Improved statistical multifragmentation (ISMM) model calculations [31] and the expanding emitting source (EES) model [32], they concluded that the difference reflects a dynamical emission process; that is, an early surface emission of isotopes during the expansion and cooling process, before the system attains thermal equilibration.

One of the complications one has to face in the study of the multifragmentation process in intermediate heavy ion reactions originates from the secondary cooling process. When fragments are formed, many of them are in excited states and cool by evaporation processes before they are detected. These secondary cooling processes may also significantly alter the information of the hot nuclear matter, carried by the primary fragments [33–35]. Even though the statistical decay process itself is rather well understood and well coded, it is not a trivial task to combine it with a dynamical code. The statistical evaporation codes assume nuclei at thermal equilibrium with normal nuclear densities and shapes. These conditions are not guaranteed in the multifragmentation process at the time that the statistical decay is invoked in the model calculation. Therefore it is desirable to investigate the primary fragments experimentally to compare their characteristic properties directly to those of the models. As a first step, in this article we report on the reconstruction of the excitation energies of the primary fragments. In order to achieve our goal, a kinematical focusing technique was employed. Using this method we extract details on neutron and light charged particle multiplicities associated with isotopically identified IMF isotopes. With the extracted multiplicities, the excitation energies are reconstructed for the parent isotopes. The determination of parameters for neutrons is more difficult than for charged particles. In addition to the fact that there is no Coulomb acceleration of the neutrons, the neutron detection itself is a difficult task. With the extracted multiplicities, the excitation energies are reconstructed for the parent isotopes.

II. EXPERIMENT

The experiment was performed at the K-500 superconducting cyclotron facility at Texas A&M University. ^{64,70}Zn and ^{64}Ni beams were used to irradiate ^{58,64}Ni, ^{112,124}Sn, ^{197}Au, and ^{232}Th targets at 40 MeV/nucleon. In this article, we focus on the ^{64}Zn + ^{112}Sn reaction, which had the best statistical precision. Intermediate mass fragments (IMFs) were detected by a detector telescope placed at $\theta_{\rm lab} = 20^o$. This telescope provided the main trigger for all detected events. As discussed in detail in Ref. [34], the events measured by this IMF trigger belong essentially to the event class of semicentral collisions. The telescope consisted of four Si detectors. Each Si detector had an effective area of 5 × 5 cm. The nominal detector thicknesses were 129, 300, 1000, and 1000 μm. All Si detectors were segmented into four sections and each quadrant subtended a 5^o polar angle. For atomic numbers Z up to $Z = 18$, six to eight isotopes were typically clearly identified using the $\Delta E \times E$ technique for any two consecutive detectors. Mass identification of the isotopes was made using a range-energy table [36]. The energy thresholds were 4 to 10 MeV/nucleon, from Li isotopes to the heaviest isotopes identified.

In Fermi energy heavy ion collisions, light particles (LPs) are emitted at different stages and from different sources during the evolution of the collision. In the following the particles not emitted from the precursor primary fragment of the detected IMF are designated as uncorrelated particles, and those emitted from the precursor fragment are called correlated particles. One should note that, according to the results of AMD-GEMINI simulations, the majority of light particles emitted in this energy domain are uncorrelated ones. In order to determine the multiplicities of light particles associated with the observed IMFs, a kinematical focusing method was employed. When particles are emitted from a moving parent of an IMF, whose velocity is approximated by the velocity of the trigger IMF, $v_{\rm IMF}$, the particles tend to be emitted into a cone centered along the $v_{\rm IMF}$ vector. The opening angle of the cone depends on the velocities of the particles, v_p, relative to $v_{\rm IMF}$. v_p is the velocity of the particle in the rest frame of the IMF. The smaller the particle velocity, the sharper the kinematical focusing. When v_p becomes larger, the focusing is weaker, and for $v_p > v_{\rm IMF}$ the particle can be emitted into 4π.

In order to detect the light particles, two sets of detectors were used. For the light charged particles (LCPs), 16 single-crystal CsI(Tl) detectors of 3 cm length were set around the target at angles between $\theta_{\rm Lab} = 27^o$ and 155^o, tilted 30^o in the azimuthal angle to avoid shadowing the neutron detectors described below. The light output from each detector was read by a photomultiplier tube. The pulse shape discrimination method was used to identify p, d, t, h, and α particles. The energy calibrations for these particles were performed using Si detectors of 50 to 300 μm in front of the CsI detectors in a separate run.

For neutrons 16 detectors of the Belgian-French neutron detector array, DEMON (Detecteur Modulaire de Neutrons) [37], were used. Eight of them were set in the plane perpendicular to the reaction plane. The zero degree in polar and azimuthal angles of the opening angle was taken to be the telescope direction. The reaction plane is defined by the vector of the telescope direction and that of the beam. The other eight neutron detectors were set in the reaction plane as shown in Fig. 1. DEMON detectors utilize a 20 cm long cell, with a diameter of 16 cm, that contains 4.5 liters of liquid scintillator (NE213). The DEMON and CsI detectors were distributed to achieve opening angles of $15^o \leqslant \theta_{\text{IMF-}n} \leqslant 160^o$ between the

FIG. 1. (Color online) DEMON detector setup viewed from upstream of the beam. In the spherical scattering chamber, the IMF telescope and 16 CsI detectors were arranged around the target. The figure has not been digitally altered.

telescope and the DEMON detectors and $17^o \leqslant \theta_{\text{IMF-}p} \leqslant 157^o$ between the telescope and the CsI detectors.

In DEMON detectors, neutron/gamma discrimination was obtained by a pulse shape analysis comparison of the slow component of the light output to the total light output. While the default distance in the DEMON setup [37] was ~ 2 m, we used flight distances of 1–1.2 m in order to increase the event rate. When the detector-target distance becomes shorter, more neutrons emerge through the side wall, instead of going out through the back surface of the detector, and therefore the effective thickness of the detector decreases. This change caused a significant reduction of the total neutron efficiency, compared to the efficiency ϵ_0 which is measured in the center of the detector. This effect was simulated using a GEANT simulation [38]. In the simulation, the relative efficiency is calculated as the ratio between the efficiency averaged over the whole front surface, ϵ_{av}, and the central efficiency ϵ_0. ϵ_{av} decreases about 25%–30%, compared to ϵ_0 at a given neutron energy. The ratio $R = \epsilon_{av}/\epsilon_0$ also depends slightly on the neutron energy. The extracted neutron multiplicity, obtained in this experiment with the average efficiency ($\epsilon_0 R$) for the ^{64}Zn + ^{112}Sn at 40 MeV/nucleon, was in good agreement with that extracted from the NIMROD detection system in a separate run, where the average neutron multiplicity was extracted from the neutron ball. An AMD-GEMINI simulation also gives a similar results for total neutron multiplicities [38].

III. DATA ANALYSIS

In order to extract the light particle multiplicities associated with an isotopically identified IMF, it is necessary to determine the contribution of the uncorrelated particles from other sources. The uncorrelated particles are emitted from a variety of sources moving, on the average, along the beam direction. The kinematically focused correlated particles can be observed as an excess above the uncorrelated spectrum. The excess increases as the opening angle $\theta_{\text{IMF-}n}$ becomes smaller. At the same time the average velocity of the correlated particles increases in proportion to v_{IMF}. These effects are enhanced when the particle velocity is small. The correlated and uncorrelated particles can be modeled by two moving sources: one for the uncorrelated ones, moving along the beam direction, and the other moving in the IMF direction. The uncorrelated source can be a convolution of multiple sources, such as projectile-like, intermediate velocity, and target-like sources. However this method requires a lot of parameters. In the actual analysis, the uncorrelated source spectra are replaced by an experimentally observed spectrum from events which are triggered by isotopes with low associated secondary particles as a reference. Therefore the extracted multiplicity of a given isotope needs to be increased by an amount corresponding to that of the correlated particle emission from the reference isotope. This is done using results of the AMD-GEMINI simulation described below.

Under this assumption, the shape of the uncorrelated spectrum was obtained from the velocity spectrum in coincidence with Li isotopes. Since the spectra in different velocity windows for different isotopes of Li are very similar to each other, the uncorrelated spectra are obtained by averaging over all available spectra in the different isotopes and in the different velocity windows.

The contribution of the correlated particles is determined using a moving source parametrization of a single source [39]. In the actual application, the IMF velocity spectrum was divided into three parts: $3.5 < v_{\text{IMF}} \leqslant 4.5$ cm/ns, $4.5 < v_{\text{IMF}} \leqslant 5.5$ cm/ns, and $5.5 < v_{\text{IMF}} \leqslant 6.5$ cm/ns. In each velocity window, the velocity spectra of the associated light particles were examined. The velocity of the moving source of the correlated particles is taken as v_{IMF}. Since the uncorrelated spectra may differ for different trigger isotopes, they are determined from that of Li isotopes multiplied by a factor k. The k value is optimized for a given isotope from the spectra observed at $\theta_{\text{IMF-}n} \geqslant 50^o$ where the correlated particle contribution is negligible. A surface Maxwellian emission with three source parameters, the multiplicity M, the temperature T, and the Coulomb barrier E_c, was assumed to model the velocity spectra of all light particles in coincidence with a given isotope. Three parameters were searched for the different IMF velocity windows. Typical results for neutrons and protons are shown in Figs. 2 and 3. Velocity spectra at four of the smallest opening angles $\theta_{\text{IMF-}n}$ for neutrons in coincidence with ^{23}Na and for protons in coincidence with ^{24}Mg are shown together with results of the calculations.

For neutrons, one can clearly see the kinematical focusing effect. The angular distribution of the correlated spectra (dashed histograms) becomes more focused on the IMF direction when the IMF velocity increases from the top to the bottom of Fig. 2. At the same time, the peak velocity increases as the IMF velocity increases. At the top left, the peak velocity is around 5 cm/ns and it increases to 6.5 cm/ns at the bottom left. These effects are weaker in the proton case because of the higher energies, reflecting Coulomb energy acceleration and higher emission temperature parameters.

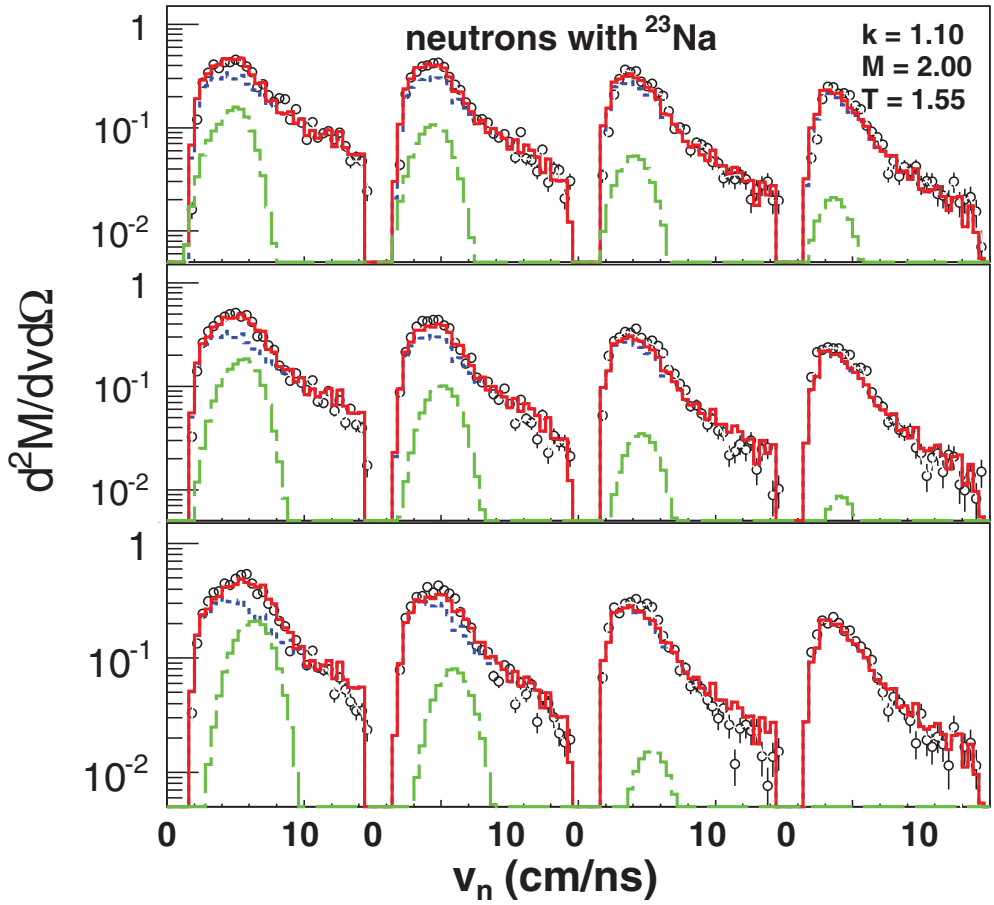

FIG. 2. (Color online) Neutron multiplicity as a function of velocity in coincidence with ^{23}Na in the velocity windows of $3.5 < v_{\rm IMF} \leqslant 4.5$ cm/ns (top), $4.5 < v_{\rm IMF} \leqslant 5.5$ cm/ns (middle), and $5.5 < v_{\rm IMF} \leqslant 6.5$ cm/ns (bottom). The double differential multiplicity is given in an absolute scale of $(\text{cm/ns})^{-1}$. Spectra from left to right in each row correspond to opening angles of $\theta_{\text{IMF-}n} = 15^\circ$, 25°, 35°, and 45°, respectively. Open circles represent experimental data. Dotted, dashed, and solid histograms correspond to the calculated spectrum of uncorrelated neutrons, correlated neutrons, and the sum of the two, respectively. The extracted k, M, and T values are also shown.

A. Neutrons

The extracted parameters k, M, and T for neutrons are summarized in Fig. 4. The k values were determined, independently of the moving source parameters, from the spectra with $\theta_{\text{IMF-}n} \geqslant 50^o$ in which the correlated neutron contribution is negligible. The extracted k values show a slight increase from $k = 1.0$ to $k = 1.1$ as A increases. M and T values are determined from the spectra with $\theta_{\text{IMF-}n} < 50^o$ using the fixed k value. Within the error bars, no notable differences are observed between the spectra perpendicular to the reaction plane and those in the reaction plane, and therefore the same parameters are used for all spectra. The extracted apparent temperature values, T, show values $T = 1.50$ to 1.75 MeV. The values for the lighter isotopes with $A < 15$ ware often not determined because of the low statistics for the correlated neutrons. In those cases T from the neighboring isotopes was used to extract the M value and an error of ± 0.25 MeV is assigned to T. This is the maximum error value of the searched value for the other cases. The extracted neutron multiplicity generally increases as Z increases. On the other hand, for a given Z the multiplicity tends to decrease as the isotopic mass A increases, except for a few cases.

The extracted neutron multiplicities are further compared to those from the neutron ball experiment and the calculations [38]. The total neutron multiplicity from this analysis is calculated as

$$M_{\rm tot} = kM_{\rm Li} + M_{\rm corr}(Z). \quad (1)$$

$M_{\rm Li}$ is the average neutron multiplicity for Li. $M_{\rm Li}$ was evaluated by a moving source fit with three sources from the neutron spectra in coincidence with Li isotopes, which results in $M_{\rm Li} = 18.3$. $M_{\rm corr}(Z)$ is an average value of the correlated neutron multiplicity, which is calculated as the IMF-multiplicity weighted average value, averaged over the values of the observed isotopes for a given Z in the top right of Fig. 4. The calculated total neutron multiplicity of Eq. (1) is shown in Fig. 5, together with those from the neutron ball and AMD-GEMINI calculations. The neutron multiplicities from the neutron ball show a trend similar to those obtained in this analysis, but the multiplicities are about 1–2 neutrons larger. The results from the AMD-GEMINI calculation are also consistent.

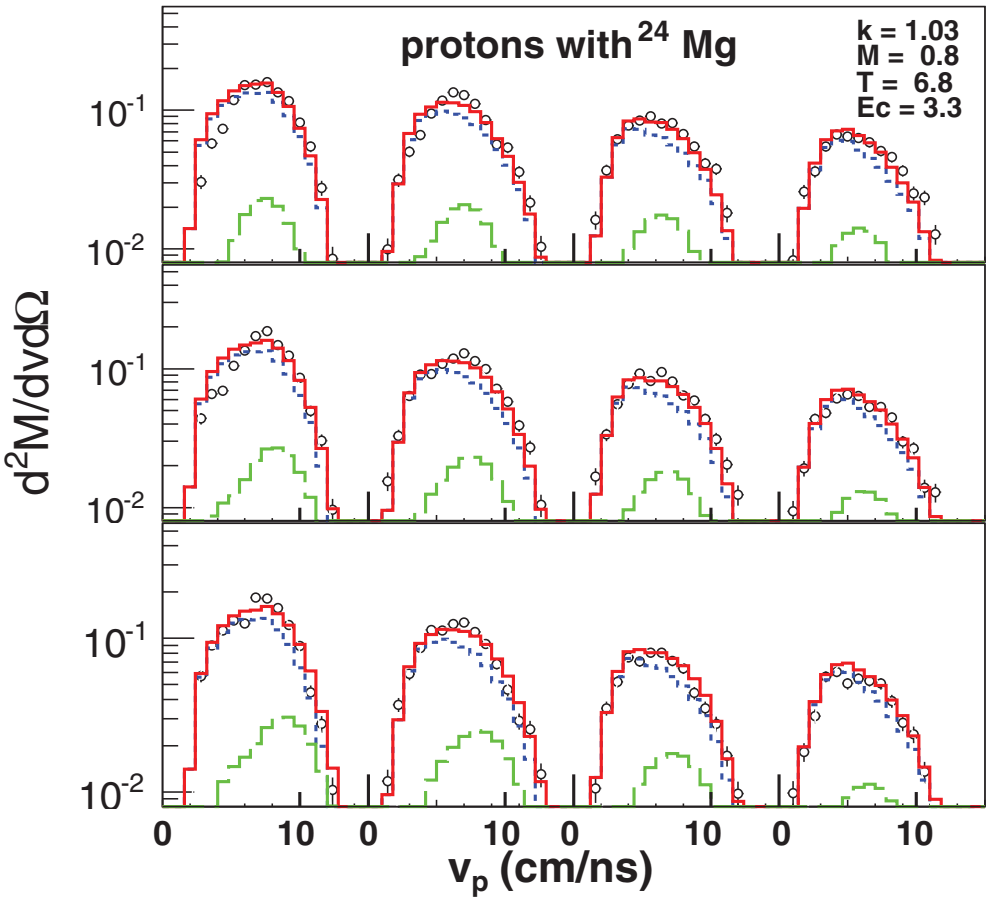

FIG. 3. (Color online) Proton multiplicity as a function of velocity in coincidence with ^{24}Mg. The double differential multiplicity is given in an absolute scale of $(\mathrm{cm/ns})^{-1}$. Spectra from left to right in each row correspond to the opening angles of $\theta_{\mathrm{IMF}\text{-}n} = 17^\circ$, 27°, 37°, and 47°, respectively. Symbols and lines are the same as those in Fig .2.

B. Charged particles

The extracted parameters for correlated proton emissions are shown in Fig. 6. The extracted k values are similar to those for neutrons. A large difference is observed in the apparent temperature T. For the lighter isotopes, $T \sim 10$ MeV was required. T decreases gradually as A increases, and becomes $T \sim 6$ MeV for $A \sim 30$. The extracted multiplicities show a similar trend to that of neutrons, but the values are about three times smaller.

The extracted parameters are compared to those in Refs. [40,41]. Our multiplicity values are about twice larger than those in Refs. [40,41]. The extracted apparent temperatures are also quite different. The temperatures in Ref. [40] show no significant Z dependence and $T = 2$–4 MeV between $Z = 4$ and 20. Note that, since only Z identification of IMFs was made in Refs. [40,41], their values are the multiplicity-weighted average value over the observed isotopes for a given Z, and fluctuate rather widely along the lines. $A = 2Z$ is assumed for the comparison with our results.

The extracted parameters for α particles are shown in Fig. 7. The k values also show a tight distribution around 1. The T values decrease from 6 to 4 MeV as the isotope mass increases. The extracted multiplicities show a rather flat distribution as a function of Z, but exhibit a similar decreasing trend as A decreases for a given Z. In contrast to the proton results the extracted values are about two times smaller than those of Refs. [40,41], as shown by the lines. The T values in Ref. [40] are around 4–6 MeV, a range similar to the present results, and they do not show a Z dependence.

The extracted parameters for deuterons and tritons are shown in Figs. 8 and 9. The k values show a slightly wider spread around 1, because of the lower statistics. For the deuteron case, the T values were not well determined and needed to be fixed at 10 MeV for more than a half of the cases. For the triton case, the extracted T values are around 6 to 9 MeV, and no significant trend was observed as a function of A. In both cases, the extracted multiplicities show clear trends, similar to those observed for protons. The multiplicity increases as Z increases, but it decreases as A increases for a given Z. The extracted values in this work are similar to the values of Refs. [40,41]. The multiplicities of ^{3}He were not determined because of poor statistics for the correlated yield.

There are significant differences in the extracted charged particle parameters between our results and those in Refs. [40,41]. Extraction techniques are different. In both cases the evaluation of the uncorrelated particle contribution is a crucial factor, because the majority of the associated

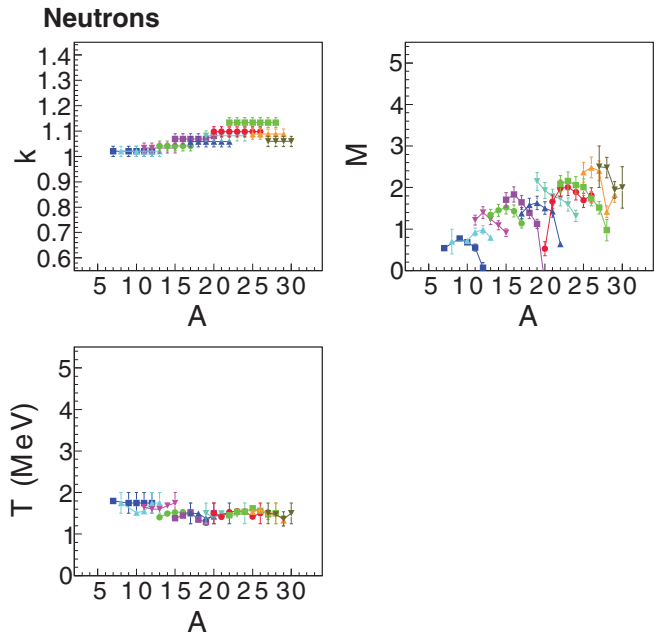

FIG. 4. (Color online) Extracted k (top left), M (top right), and T (bottom) values for neutrons as a function of the mass of triggered isotopes. Results for a given Z value are connected by lines, and different symbols are used for different Z values of isotopes. The symbols correspond to Be (blue squares), B (light blue triangles), C (magenta triangle), N (green dots), O (magenta squares), F (blue triangles), Ne (light green diamonds), Na (red dots), Mg (green squares), Al (yellow triangles), and Si (grey triangles).

particles are uncorrelated ones. In Refs. [40,41], the central collisions of ^{129}Xe + Sn were studied at the incident energies between 32 and 50 MeV/nucleon. The light charged particle multiplicities (LCPs) associated with IMFs of a given Z value were extracted using the yields observed as a Coulomb ring around the precursor IMF in the IMF rest frame. The reasons for the differences between our results and those in Refs. [40,41] are not clear at this moment. For the evaluation

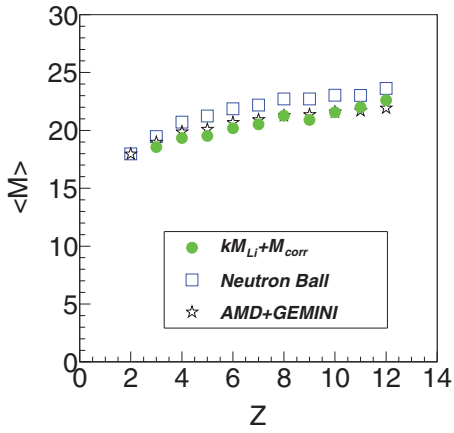

FIG. 5. (Color online) Comparisons of total neutron multiplicity obtained from this work (dots), neutron ball measurement (squares), and AMD-GEMINI calculation (stars). The latter two results are taken from Ref. [38].

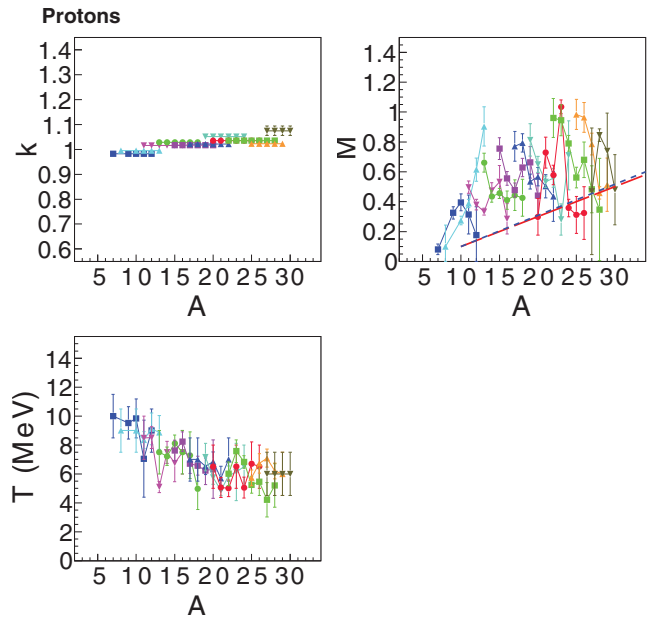

FIG. 6. (Color online) Plots similar to those in Fig. 4, but for protons. In the upper right panel, the results from Ref. [41] at 39 MeV/nucleon are shown by a dashed line and those from Ref. [40] are shown by a long-dashed line. See details in the text.

of the uncorrelated background the velocity spectrum of a charged particle of a given type in the rest frame of a precursor IMF was constructed from actual events. The background spectrum was determined from two separate uncorrelated events, the charged particle in one event and the IMF from the other, with the same central collision requirement. In this work we evaluated the uncorrelated contribution from the experimental spectra associated with Li isotopes and

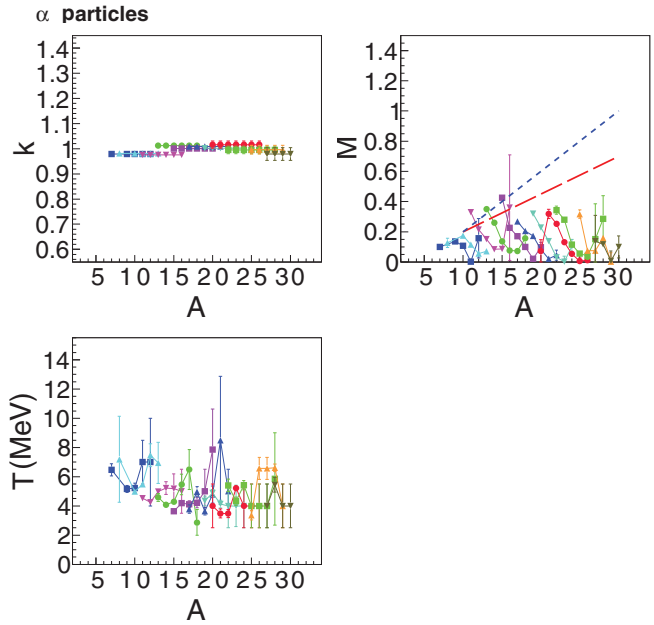

FIG. 7. (Color online) Plots similar to those in Fig. 6, but for α particles.

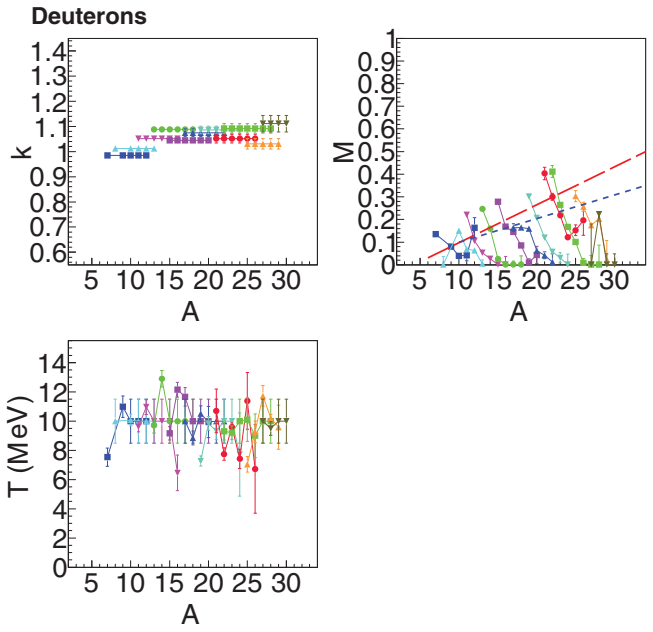

FIG. 8. (Color online) Plots similar to those in Fig. 6, but for deuterons.

used a free parameter k to account for the slight difference of the uncorrelated yield for different precursor IMFs. The evaluation of the uncorrelated background in our method is straightforward and somewhat less model dependent, but the excess yield above the uncorrelated background is less prominent than those in the Coulomb ring method, because it spreads over several spectra as seen in Fig. 3. In order to compare the two methods, further systematic studies are needed. While the difference in technique might have some effect on the results, we believe that the main differences reflect

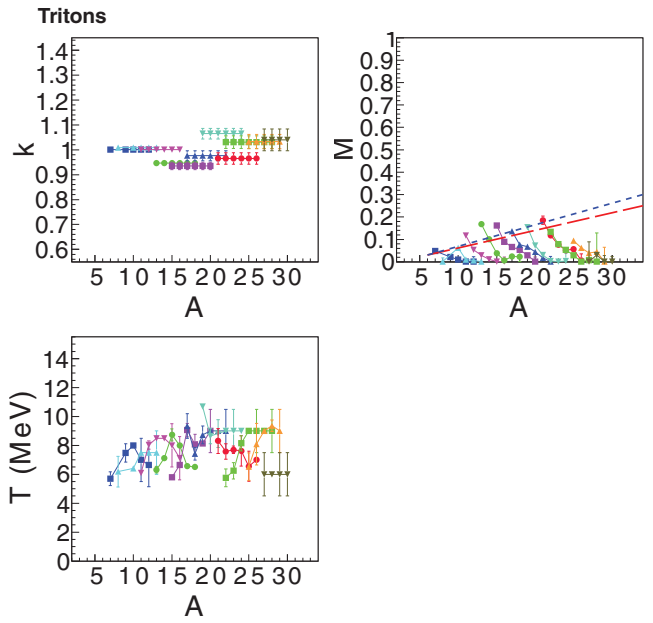

FIG. 9. (Color online) Plots similar to those in Fig. 6, but for tritons.

the differences inherent in the event selection and degree of equilibration achieved in the selected events.

IV. EXCITATION ENERGY AND DISCUSSION

From the extracted multiplicities in the previous section, the excitation energies of the primary isotopes are evaluated. The excitation energy is given in energy per nucleon. As mentioned earlier, the experimentally determined values of the correlated LP multiplicities are relative to those of Li isotopes and need to be corrected by adding an amount to each multiplicity, corresponding to that of emission from the Li isotopes. The amounts are obtained from the AMD-GEMINI simulation [12,42], by extracting the average multiplicity of each LP over all Li isotopes. Calculations with different equations of state (hard and soft) and different versions (AMD/DD in [12] and AMD/DS in [13]) were made. All these calculations show similar values for the LP multiplicities emitted from the Li isotopes. The amounts extracted are 0.40 ± 0.05 for the neutrons, 0.24 ± 0.04 for protons, 0.044 ± 0.005 for deuterons, 0.035 ± 0.005 for tritons, and 0.32 ± 0.04 for α particles. These values are added to the experimentally extracted LP multiplicities obtained for the other isotopes.

With these values, the average excitation energies of the primary fragments are calculated using a Monte Carlo method. Since the experimental values are the average values, one needs to evaluate the shape of the multiplicity distributions for use in the Monte Carlo method. This was done using GEMINI simulations [42]. The mass range of isotopes for parent nuclei was determined from the AMD simulation. For each parent nucleus with a given excitation energy, 100 000 deexcitation events were generated. Since only the shape of the associated LP multiplicity distributions was required, a uniform yield distribution for all parent nuclei was assumed. The associated LP multiplicity distributions were generated and the shapes fit by assuming a Gaussian form. The extracted centroid and width σ are stored in a database as a function of A and Z of the cold fragment. The database was generated for the excitation energy range from 1 to 5 MeV/nucleon.

The LP multiplicities, M_i $(i = n, p, d, t, \alpha)$, are generated for a given cold daughter nucleus on an event-by-event basis. For a given width of the Gaussian distribution, the centroid of the distribution is adjusted to give the same average multiplicity as that of the experiment. Then the excitation energy of the primary isotopes, $E_X(A_{\rm hot}, Z_{\rm hot})$, is calculated as

$$E_X(A_{\rm hot}, Z_{\rm hot}) = \sum_i \langle E_i \rangle\, M_i + Q + E_\gamma. \qquad (2)$$

$\langle E_i \rangle$ is the average kinetic energy of the particle i and it is evaluated from the moving source fit parameter T as $\langle E_i \rangle = 2T$. Q is the reaction Q value. E_γ is the average energy carried away by gamma emission, and was evaluated from the AMD-GEMINI calculation [12,43]. The experimental results are shown in Fig. 10, using the database values of 2.5 MeV/nucleon in (a) and 1.5 MeV/nucleon in (b). The choice of the database values among those corresponding to $E_x = 1$ to 5 MeV/nucleon was made in such a way that

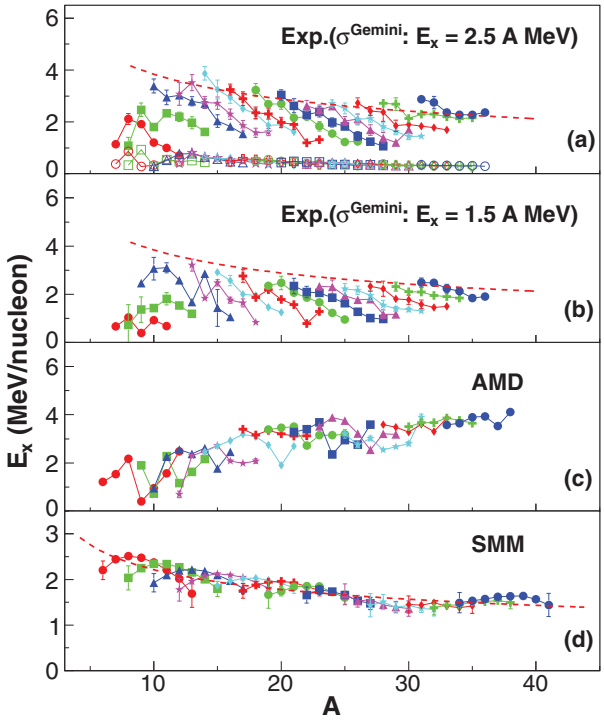

FIG. 10. (Color online) Excitation energies of the primary hot nuclei with $Z \geqslant 4$ as a function of the mass A of the primary hot isotopes, evaluated from (a) the experiment with σ from the 2.5 MeV/nucleon database, (b) the experiment with σ from the 1.5 MeV/nucleon database, (c) AMD, and (d) SMM. The same symbols are used for each isotope of a given element. In (a), the calculated average E_γ are also shown by open symbols, together with the total excitation energy (solid symbols). The symbols correspond to Be (red circles), B (green squares), C (blue triangles), N (magenta stars), O (light blue diamonds), F (red crosses), Ne (green circles), Na (blue squares), Mg (magenta triangles), Al (light blue stars), Si (red diamonds), P (green crosses), and S (blue circles).

the reconstructed primary fragment excitation energies in Fig. 10 are globally consistent with that initial excitation energy. The total reconstructed excitation energies of the primary hot nuclei are shown by closed symbols and those of the calculated average E_γ are shown by open symbols in Fig. 10(a). There are some notable differences for the extracted excitation energies in the top two figures. For widths consistent with $E_x = 2.5$ MeV/nucleon the average excitation energy is around 2–3 MeV/nucleon, and for widths consistent with $E_x = 1.5$ MeV/nucleon it becomes around 1.5–2.5 MeV/nucleon. There is a significant spread around these values. However, the trends of the reconstructed energies in both cases are very similar to each other. In both cases the excitation energies for the isotopes with $Z = 4$ and 5 are low and show a different trend from that of the other isotopes. For $Z \geqslant 6$ the excitation energies are largest for the most neutron deficient isotopes and decrease gradually as A increases from 10 to 36 at a rate approximately proportional to $A^{-1/3}$, as indicated by dashed curves in both panels.

The errors of these extracted values are evaluated, taking into account uncertainties in the temperature and the multiplicity. In both cases the errors are dominated by the systematic errors for the moving source fit and they are evaluated as 10% in the multiplicity and 0.25 MeV in the temperature. When the errors from the multiplicity are evaluated, the errors in the amount added for the correction of the emission from the Li isotopes (Li offset) are also taken into account besides the systematic error of the multiplicity, using root-mean-square values. One should note that, in the reconstruction of the excitation energy, the neutron multiplicity makes the major contribution and therefore the errors associated with the neutron emission parameters dominate the errors in the excitation energy. Since the errors are dominated by the systematic errors, the errors $\Delta E_X^Y(A_{\rm hot}, Z_{\rm hot})$ ($Y = T$ for the temperature and $Y = M$ for the multiplicity) are simply calculated as

$$\Delta E_X^Y(A_{\rm hot}, Z_{\rm hot}) = [E_X(A_{\rm hot}, Z_{\rm hot}, Y + \Delta Y) - E_X(A_{\rm hot}, Z_{\rm hot}, Y - \Delta Y)]/2. \quad (3)$$

For the multiplicity, Y is the multiplicity after the correction of the Li offset and ΔY is the error from the multiplicity and the Li offset. Assuming the errors in T and M are independent, the total errors in the reconstructed excitation energies are calculated as the mean-square value of $\Delta E_X^T(A_{\rm hot}, Z_{\rm hot})$ and $\Delta E_X^M(A_{\rm hot}, Z_{\rm hot})$ and are used in Figs. 10(a) and 10(b). Typical error values for ^{12}C in Fig. 10(a) are $\Delta E_X^M \sim 0.16$ MeV, $\Delta E_X^T \sim 0.05$ MeV, and the total error $\Delta E_X \sim 0.17$ MeV. The error contribution from the multiplicity becomes larger partially because the contribution comes from the first term and Q value term in Eq. (2).

The extracted excitation energies may be compared to those of dynamical and statistical model simulations. The models used are the antisymmetrized molecular dynamics (AMD) of Ono *et al.* [11,12] and the statistical multifragmentation model (SMM) of Bondorf *et al.* [3,4]. In the AMD simulation, the ^{64}Zn + ^{112}Sn reaction at 40 MeV/nucleon is simulated with the Gogny interaction. The excitation energies of the primary hot nuclei are evaluated at $t = 300$ fm/c. The results are shown in Fig. 10(c). In general the calculated excitation energies increase as A increases for a given Z. This increasing trend is in clear contrast to that of the experimental results. However, the majority of the excitation energies of the isotopes with $A \leqslant 20$ are reasonably consistent with those of the experiment, except for those of the very neutron deficient isotopes.

For the SMM simulation, $A = 60$, $Z = 26$, $E_x = 3$ MeV/nucleon, and $\rho = 0.25\rho_o$ are used. The size of the fragmenting source is evaluated from the NN source multiplicities of all particles, determined by a moving source fit described in Ref. [34,44]. The excitation energy of the fragmenting system is chosen to give an average value roughly similar to those of the experiment. In the SMM, the excitation energy of the fragments with $A_{\rm hot}$, $Z_{\rm hot}$ is given by [4]

$$E_X(A_{\rm hot}, Z_{\rm hot}) = T^2/\epsilon + \left(\beta(T) - T\frac{d\beta(T)}{dT} - \beta_o\right) A^{-1/3}. \quad (4)$$

The first term is from the bulk free energy. $\epsilon = A/a$ and a is the level density parameter. The second term is from the surface free energy; $\beta(T)$ is the surface energy coefficient at T and $\beta_o = \beta(T = 0) = 18$ MeV. The results are shown in Fig. 10(d). The excitation energy decreases smoothly as

A increases. This decrease originates from the second term of Eq. (4) and the rate is proportional to $A^{-1/3}$, indicated by the dashed line, which is similar to that observed in the experimental results for the most or near neutron deficient isotopes with $A > 10$ in the top two panels. However, in the SMM all isotopes follow this trend. In the SMM calculations, the parameters of the initial condition change the absolute values of the excitation energies, but the essential features, such as the smooth decreasing trend and no notable structure among isotopes for a given Z, remain the same.

In the above comparisons, one should note that the experimental values are for the primary hot fragments which decay into one IMF + LPs channels, whereas in the model calculations the primary fragments of other possible decay channels, such as two IMFs + LPs, if any, are included. However, in the experiment another $Z = 3$ fragment associated with the precursor isotope was also measured by the CsI detectors, and its multiplicity was much smaller than the multiplicity of d, t, and ^{3}He. Therefore we concluded that the contribution of the multiple IMFs + LPs decay channels is negligible. This is consistent with the SMM calculations, which showed that one IMF + LPs decay channels dominate when the reconstructed excitation energy in Fig. 10(a) was given to each parent isotopes. Lighter primary isotopes may decay into channels in which no IMF remains. The excitation energies of the primary isotopes in such decay channels were not reconstructed in this work.

The extracted temperatures of the LPs are quite different. The source temperature of the primary isotope with an excitation energy of 1.5–4 MeV/nucleon is expected to be about $T = 3.5$–5.6 MeV, if one uses $T = \sqrt{E/a}$. The measured neutron temperatures are around 1.5–1.75 MeV. However, one should note that in most cases the multiplicity of the neutrons is more than two, and therefore the apparent temperature becomes an average over cooling cascades [45] and the temperature is lowered. The temperature of protons is 6 to 10 MeV and that of α particles is 4 to 6 MeV. The charged particles tends to be emitted early in the cascade and their temperatures are expected to be near 3.5 to 4 MeV/nucleon. However, in this study the statistics is rather low, especially for the charged particles, and therefore it is difficult to pursue the observed differences any further. Within this limitation, the extracted apparent temperatures were only used to calculate the mean kinetic energies of the ejectiles from the primary hot source in Eq. (2).

For isotopes with $A < 20$, the AMD model predicts reasonable values except for those of the very neutron deficient ones. On the other hand, the experimental values for the very neutron deficient isotopes decrease proportional to $A^{-1/3}$, the same rate as that predicted in the SMM. For the other isotopes with $A \geqslant 20$ the excitation energies tend to decrease as A increases, which is also consistent with SMM predictions. These observations suggest that the isotopes with $A < 20$ are emitted mainly in a dynamical process before thermal equilibration is attained, and those with $A \geqslant 20$ are emitted after a greater degree of the thermal and chemical equilibrium is attained. The higher excitation energies for the very neutron deficient isotopes may reflect the mechanism reported by Liu *et al.* [30], in which these isotopes are emitted early. Further, more detailed experiments and model simulations are necessary to verify this.

V. SUMMARY

A kinematical focusing method is employed to determine the multiplicities of light particles evaporated from the hot primary isotopes produced in ^{64}Zn + ^{112}Sn reactions at 40 MeV/nucleon. A moving source fit was employed to extract the multiplicities of kinematically correlated light particles (n, p, d, t, and α particles) associated with triggered isotopes. In general the extracted multiplicities of all LPs increase as Z of the isotope increases and, for a given Z, decrease as A of the isotope increases. The latter trend is enhanced for the charged particles, though the absolute multiplicities are much smaller than those of neutrons. The excitation energies of the primary hot isotopes were reconstructed by a Monte Carlo method, using the shape of the multiplicity distributions and the average energies carried away by gamma emission (determined from GEMINI simulations).

In order to reconstruct the excitation energy of the primary fragments, the neutron measurements play a crucial role. The extracted excitation energies show the largest values for the most neutron deficient isotopes and decrease significantly as A increases for a given Z. The largest values of the excitation energy derived for each Z decrease as $A^{-1/3}$. The comparisons between the experimental values and those of the model simulation suggest that the isotopes with $A < 20$ are mainly produced dynamically before the thermal equilibration is attained and those with $A \geqslant 20$ are emitted after a greater degree of the thermal and chemical equilibrium is attained.

ACKNOWLEDGMENTS

We thank the staff of the Texas A&M Cyclotron facility for their support during the experiment. We thank the Institute of Nuclear Physics of the University of Louvain and Prof. Y. El Masri for allowing us to use the DEMON detectors. We thank A. Ono and R. J. Charity for providing their codes. This work is supported by the US Department of Energy under Grant No. DE-FG03-93ER40773 and the Robert A. Welch Foundation under Grant No. A0330. This work is also supported by the National Natural Science Foundation of China (Grant No. 11075189) and 100 Persons Project (No. 0910020BR0 and No. Y010110BR0), and by ADS Project 302 (No. Y103010ADS) of the Chinese Academy of Sciences.

[1] D. H. E. Gross, Rep. Prog. Phys. **53**, 605 (1990).
[2] M. D'Agostino *et al.*, Nucl. Phys. A **650**, 329 (1999).
[3] J. P. Bondorf, R. Donangelo, and I. N. Mishustin, Nucl. Phys. A **443**, 321 (1985).

[4] J. Bondorf, A. S. Botvina, A. S. Iljinov, I. N. Mishutin, and K. Sneppen, Phys. Rep. **257**, 133 (1995).
[5] A. S. Botvina *et al.*, Nucl. Phys. A **584**, 737 (1995).
[6] M. D'Agostino *et al.*, Phys. Lett. B **371**, 175 (1996).
[7] R. P. Scharenberg *et al.*, Phys. Rev. C **64**, 054602 (2001).
[8] N. Bellaize *et al.*, Nucl. Phys. A **709**, 367 (2002).
[9] S. P. Avdeyev *et al.*, Nucl. Phys. A **709**, 392 (2002).
[10] R. Ogul *et al.*, Phys. Rev. C **83**, 024608 (2011).
[11] A. Ono and H. Horiuchi, Phys. Rev. C **53**, 2958 (1996).
[12] A. Ono, Phys. Rev. C **59**, 853 (1999).
[13] A. Ono, S. Hudan, A. Chbihi, and J. D. Frankland, Phys. Rev. C **66**, 014603 (2002).
[14] A. Ono and H. Horiuchi, Prog. Part. Nucl. Phys. **53**, 501 (2004).
[15] R. Wada *et al.*, Phys. Lett. B **422**, 6 (1998).
[16] R. Wada *et al.*, Phys. Rev. C **62**, 034601 (2000).
[17] R. Wada *et al.*, Phys. Rev. C **69**, 044610 (2004).
[18] S. Hudan, R. T. de Souza, and A. Ono, Phys. Rev. C **73**, 054602 (2006).
[19] M. Colonna, M. Di Toro, A. Guarnera, S. Maccarone, M. Zielinska-Pfabe, and H. H. Wolter, Nucl. Phys. A **642**, 449 (1998).
[20] V. Baran, M. Colonna, M. Di Toro and R. Zus, Phys. Rev. C **85**, 054611 (2012).
[21] F. Gagnon-Moisan *et al.*, Phys. Rev. C **86**, 044617 (2012).
[22] N. Wang, Z. Li, and X. Wu, Phys. Rev. C **65**, 064608 (2002).
[23] N. Wang, Z. Li, X. Wu, J. Tian, Y. X. Zhang, and M. Liu, Phys. Rev. C **69**, 034608 (2004).
[24] Y. Zhang and Z. Li, Phys. Rev. C **71**, 024604 (2005).
[25] Y. Zhang and Z. Li, Phys. Rev. C **74**, 014602 (2006).
[26] Y. Zhang *et al.*, Phys. Rev. C **85**, 024602 (2012).
[27] A. H. Raduta, M. Colonna, V. Baran and M. Di Toro, Phys. Rev. C **74**, 034604 (2006).
[28] A. H. Raduta, M. Colonna, and M. Di Toro, Phys. Rev. C **76**, 024602 (2007).
[29] T. Furuta and A. Ono, Phys. Rev. C **79**, 014608 (2009).
[30] T. X. Liu *et al.*, Europhys. Lett. **74**, 806 (2006).
[31] W. P. Tan, S. R. Souza, R. J. Charity, R. Donangelo, W. G. Lynch, and M. B. Tsang, Phys. Rev. C **68**, 034609 (2003).
[32] W. A. Friedman, Phys. Rev. C **42**, 667 (1990).
[33] M. Huang *et al.*, Phys. Rev. C **81**, 044620 (2010).
[34] M. Huang *et al.*, Phys. Rev. C **82**, 054602 (2010).
[35] Z. Chen *et al.*, Phys. Rev. C **81**, 064613 (2010).
[36] F. Hubert, R. Bimbot, and H. Gauvin, At. Data Nucl. Data Tables **46**, 1 (1990).
[37] I. Tilquin *et al.*, Nucl. Instrum. Methods A **365**, 446 (1995).
[38] S. Zhang *et al.*, Nucl. Instrum. Methods A. **709**, 68 (2013).
[39] T. C. Awes, G. Poggi, C. K. Gelbke, B. B. Back, B. G. Glagola, H. Breuer, and V. E. Viola, Jr., Phys. Rev. C **24**, 89 (1981).
[40] N. Marie *et al.*, Phys. Rev. C **58**, 256 (1998).
[41] S. Hudan *et al.*, Phys. Rev. C **67**, 064613 (2003).
[42] R. J. Charity *et al.*, Nucl. Phys. A **483**, 371 (1988).
[43] R. J. Charity, GEMINI++, 2008, www.chemistry.wustl.edu/~rc/gemini++/gemini.pdf
[44] R. Wada *et al.*, in *Proceedings of the International Workshop on Nuclear Dynamics, December 16–19, 2012, Shenzhen, China* (Nuclear Technologies and Techniques, Shanghai, China, 2013).
[45] K. Hagel *et al.*, Nucl. Phys. A **486**, 429 (1988).